

Inverse Compton Contribution to the Star-Forming Extragalactic Gamma-Ray Background

Nachiketa Chakraborty and Brian D. Fields¹

Department of Astronomy, University of Illinois, Urbana, IL

ABSTRACT

Fermi has resolved several star-forming galaxies, but the vast majority of the star-forming universe is unresolved and thus contributes to the extragalactic gamma ray background (EGB). Here, we calculate the contribution from star-forming galaxies to the EGB in the *Fermi* range from 100 MeV to 100 GeV, due to inverse-Compton (IC) scattering of the interstellar photon field by cosmic-ray electrons. We first construct a one-zone model for a single star-forming galaxy, assuming supernovae power the acceleration of cosmic rays. The same IC interactions leading to gamma rays also substantially contribute to the energy loss of the high-energy cosmic-ray electrons. Consequently, a galaxy’s IC emission is determined by the relative importance of IC losses in the cosmic-ray electron energy budget (“partial calorimetry”). We use our template for galactic IC luminosity to find the cosmological contribution of star-forming galaxies to the EGB. For all of our models, we find the IC EGB contribution is almost an order of magnitude less than the peak of the emission due to cosmic-ray ion interactions (mostly pionic $p_{\text{cr}}p_{\text{ism}} \rightarrow \pi^0 \rightarrow \gamma\gamma$); even at the highest *Fermi* energies, IC is subdominant. Moreover, the flatter IC spectrum increases the high-energy signal of the pionic+IC sum, bringing it into better agreement with the EGB spectral index observed by *Fermi*. Partial calorimetry ensures that the overall IC signal is well constrained, with only modest uncertainties in the amplitude and spectral shape for plausible model choices. Partial calorimetry of cosmic-ray electrons should hold true in both normal and starburst galaxies, and thus we include starbursts in our calculation. We conclude with a brief discussion on how the pionic spectral feature and other methods can be used to measure the star-forming component of the EGB.

¹also Department of Physics, University of Illinois, Urbana, IL

1. Introduction

The window to the high-energy (> 30 MeV) gamma-ray cosmos has been open now for four decades, with measurements by OSO-3 satellite (Kraushaar et al. 1972) followed by the second Small Astronomy Satellite (SAS-2)(Fichtel et al. 1975) and the Energetic Gamma Ray Experiment Telescope (EGRET) (Sreekumar et al. 1998). These revealed the existence of a diffuse, extra-Galactic gamma ray background (EGB). More recently, the advent of the *Fermi* Gamma-Ray Space Telescope has substantially sharpened our observational view of the EGB. With better energy and angular resolution and much higher sensitivity than EGRET, *Fermi* has resolved many more gamma-ray point sources and better determined the diffuse background and its energy dependence. The EGB data are consistent with a power law of spectral index 2.41 ± 0.05 (Abdo et al. 2010f) for energies > 100 MeV.

The origin of the EGB remains an open question. A contribution from active galaxies (e.g., Strong et al. 1976a; Abdo et al. 2009; Stecker & Venters 2011; Abazajian et al. 2011) and star-forming galaxies (e.g., Strong et al. 1976b; Bignami et al. 1979; Pavlidou & Fields 2002; Fields et al. 2010; Stecker & Venters 2011; Makiya et al. 2011) is “guaranteed” in the sense that these are known, resolved extragalactic source classes that must have *unresolved* counterparts that will contribute to the EGB. Other possible EGB sources include truly diffuse emission such as dark matter annihilation (Ando et al. 2007), interactions from cosmic rays accelerated in structure formation shocks (e.g., Loeb & Waxman 2000; Miniati 2002), unresolved ordinary and millisecond pulsars (Faucher-Giguère & Loeb 2010; Geringer-Sameth & Koushiappas 2012), and even Solar-System emission from cosmic-ray interactions with Oort cloud bodies (Moskalenko & Porter 2009).

One of *Fermi*’s major achievements has been to establish external star-forming galaxies as a new class of gamma-ray sources. These detections give a global view of the gamma-ray output as a result of star-formation, complementary to the resolved but local images of the Milky Way. *Fermi* has not only detected but also spatially resolved the Large Magellanic Cloud (LMC; Abdo et al. 2010e). As anticipated (Pavlidou & Fields 2001), the SMC (Abdo et al. 2010b) and M31(Abdo et al. 2010d) have also been detected, while other normal star-forming galaxies in the Local Group (including M33) have not (Abdo et al. 2010d; Lenain & Walter 2011). Beyond the Local Group, *Fermi* has detected starbursts galaxies characterised by very high star-formation rates, as anticipated by Torres et al. (2004). *Fermi* has detected the starbursts M82 and NGC 253 (Abdo et al. 2010a) and NGC 1068 and NGC 4945 (Nolan et al. 2012).

The *Fermi* star-forming galaxies offer a qualitatively new probe of cosmic rays; they also inform and calibrate efforts such as ours to understand the EGB contribution from the vast bulk of the star-forming universe that remains *unresolved*. The LMC is the best resolved

individual system, and there the energy spectrum is consistent with pionic, while the spatial distribution can be used to study cosmic-ray propagation (Murphy et al. 2012). More broadly, the ensemble of all *Fermi* star-forming galaxies encodes information about global cosmic-ray energetics and interaction mechanisms (Persic & Rephaeli 2010; Lacki et al. 2011; Persic & Rephaeli 2012). In particular, *Fermi* reveals a strong correlation between gamma-ray luminosity L_γ and supernova rate (or equivalently star-formation rate ψ). This is expected if supernovae provide the engines of cosmic-ray acceleration. Remarkably, all star-forming galaxies detected to date can be well-fit with a single power law $L_\gamma \propto \psi^{1.4 \pm 0.3}$ (e.g., Abdo et al. 2010d).

The main mechanism of gamma ray production in star-forming galaxies is anticipated to be the same that dominates Milky Way diffuse gamma rays: pionic emission $p_{\text{cr}}p_{\text{ism}} \rightarrow pp\pi^0 \rightarrow \gamma\gamma$, arising from interactions between cosmic-ray hadrons (ions) and interstellar gas (Stecker & Venters 2011; Abdo et al. 2009; Fields et al. 2010; Strong et al. 2010). This mechanism is likely responsible for the non-linear relation between the luminosity of *Fermi* galaxies and their star-formation rate. Namely, the observed correlation is consistent with a picture (Pavlidou & Fields 2001; Fields et al. 2010; Persic & Rephaeli 2011) in which the cosmic-ray proton flux is controlled by the supernova rate, the total number of targets is set by the galaxy’s gas mass, and the gas and star-formation are linked by the Schmidt-Kennicutt relation (Kennicutt 1998).

Here, we examine the cosmological contribution of star-forming galaxies by the inverse-Compton (IC) scattering $e_{\text{cr}}\gamma_{\text{is}} \rightarrow e\gamma$ of cosmic-ray electrons on the interstellar radiation field (ISRF). In order to do so, we construct a one-zone model of a star-forming galaxy, with the IC emission normalised to the Milky Way IC emission as computed in GALPROP (Strong et al. 2010) and use this as our galaxy template.

The IC gamma rays are produced by upscattering of interstellar radiation by high-energy cosmic-ray electrons (Felten & Morrison 1963; Felten 1965; Brecher & Morrison 1967). Inverse-Compton scattering also represents an important energy loss mechanism for these electrons; the other important losses are bremsstrahlung and synchrotron. The relative importance of these losses depends on the cosmic-ray energy and on interstellar radiation and matter densities. Where inverse Compton losses dominate, the energy injected into cosmic-ray electrons is ultimately re-emitted as IC gamma-ray photons. This equality of energy loss and energy output is known as calorimetry, and was first described in the context of high-energy electrons by Felten (1965) and explored in detail for diffuse high-energy gamma rays by cosmic rays by Pohl (1994). If the other losses are negligible then we have perfect calorimetry. However, if other losses compete, the gamma-ray energy output is reduced by the IC fraction of the energy losses by the cosmic rays. As we will see, the latter holds true for the case of

Milky Way type galaxies. We can explain our results in terms of this partial calorimetry.

In contrast, cosmic-ray hadrons (mainly protons, as well as other ions) in the Milky Way suffer losses dominated by escape rather than collisions. The pionic emission from normal star-forming galaxies is thus not calorimetric; however, in starburst galaxies, proton inelastic interactions can dominate losses and lead to calorimetry (Lacki et al. 2010). In the Milky Way, pionic emission dominates the total Galactic gamma-ray output (luminosity), exceeding IC emission by factors of up to ~ 5 in GALPROP calculations (Strong et al. 2010). Our analysis shows that the inverse-Compton component from star-forming galaxies over cosmological volumes is nearly an order of magnitude lower than the peak of the pionic component.

The paper is organised as follows. Section 2 gives an order-of-magnitude estimate of the inverse Compton EGB contribution by star-forming galaxies, and serves as an overview to our paper. We first build a template for the IC emission from a star-forming galaxy, starting with the various components of the background interstellar photon field §3. These interstellar photons serve as scattering targets for the cosmic ray electrons, whose propagation is explained in §4. For the highest energy background photons and electrons, the scattering occurs in the Klein-Nishina regime, which affects the emergent spectrum and is detailed in §5.1. Our one-zone model for the inverse-Compton luminosity from a single galaxy is presented in §5.2. In §6, the total intensity over cosmological volumes is calculated and compared with the pionic component. Section 7 discusses the implications of our results.

2. Order-of-Magnitude Expectations

An order-of-magnitude estimate of our final result will help frame key physical issues and astrophysical inputs. Our goal is to find the gamma-ray specific intensity, I_E , due to inverse Compton scattering in star-forming galaxies, at energy E . For photons up to at least $\lesssim 30$ GeV, the universe is optically thin; thus, the intensity is simply given by the line-of-sight integral

$$I_E \approx \frac{c}{4\pi} \int_{\text{los}} d\ell \mathcal{L}_\gamma \approx \frac{\mathcal{L}_\gamma d_H}{4\pi} \quad (1)$$

where \mathcal{L}_γ is the luminosity density or cosmic volume emissivity of the galaxies, and $d_H = c/H_0 = 3000h^{-1}$ Mpc is the Hubble length. The total luminosity density of a distribution of IC-emitting, star-forming galaxies can be expressed as a product of the luminosity function, $dn_{\text{gal}}/dL_\gamma$ and the luminosity of each individual galaxy, L_γ :

$$\mathcal{L}_\gamma = \int L_\gamma \frac{dn_{\text{gal}}}{dL_\gamma}(L_\gamma) dL_\gamma = \langle nL_\gamma \rangle \approx n_{\text{gal}} L_E \quad (2)$$

where L_E is the luminosity of an average galaxy at energy E .

Within a single galaxy, the gamma-ray luminosity is an integral

$$L_\gamma(E_{\text{em}}) = \int q_{\text{ic}} dV_e \quad (3)$$

over the volume in which cosmic-ray electrons propagate. Here the inverse-Compton volume emissivity q_{ic} depends on the product of the targets and projectile densities, and the interaction cross section. The density of targets is simply the number density of the interstellar photons, n_{isrf} . The projectiles are cosmic-ray electrons, with flux density ϕ_e . The cross section is that for inverse Compton scattering, $d\sigma_{\text{ic}}/dE_{\text{em}}$. Therefore, the emissivity for a single galaxy is given as,

$$q_{\text{ic}} = \left\langle \phi_e \frac{d\sigma_{\text{ic}}}{dE_{\text{em}}} n_{\text{isrf}} \right\rangle \quad (4)$$

with the angle brackets indicating averaging over the cosmic-ray and background photon energies.

There is substantial evidence that cosmic-ray acceleration is powered by supernova explosions (Hayakawa et al. 1958, 1964; Uchiyama et al. 2007; Ahlers et al. 2009). Indeed, the cosmic-ray/supernova link historically has been better established for cosmic ray electrons via radio (Webber et al. 1980; Strong et al. 2011; Bringmann et al. 2012) and X-ray synchrotron (Uchiyama et al. 2007; Helder et al. 2009) measurements. Only very recently have *Fermi*-LAT (Ahlers et al. 2009) measurements of pionic gamma rays provided the most direct evidence for supernova acceleration of protons and other ions. Consequently, a galaxy's cosmic-ray injection rate is proportional to its supernova rate, $q_{\text{cr}} \propto R_{\text{SN}}$ and therefore, the galactic star-formation rate, ψ .

Cosmic-ray electron propagation is dominated by energy losses in the form of inverse Compton, bremsstrahlung and synchrotron processes. Each contributes to a total energy loss rate $b_{\text{tot}} = |dE_e/dt|$. The IC loss rate is proportional to the background photon energy density: $b_{\text{ic}} \propto U_{\text{isrf}} \propto n_{\text{isrf}}$. In steady-state, cosmic-ray losses balance their production, and thus the flux is set by the production rate q_e times the stopping time $\propto 1/b_{\text{tot}}$, giving $\phi_e \propto q_e/b_{\text{tot}}$. If IC losses dominate, then $\phi_e \propto q_e/b_{\text{ic}} \propto q_e/n_{\text{isrf}}$, and the cosmic-ray flux is *inversely* proportional to the photon density: more interstellar photons mean a shorter stopping time. More generally, the cosmic-ray flux $\phi_e \propto (b_{\text{ic}}/b_{\text{tot}}) q_e/n_{\text{isrf}}$ is *lower* by the fraction $b_{\text{ic}}/b_{\text{tot}}$ of energy losses in IC.

The galactic IC emissivity depends on the product of flux and targets: $q_{\text{ic}} \propto \phi_e n_{\text{isrf}} \propto (b_{\text{ic}}/b_{\text{tot}}) q_e$. If IC losses dominate, then $b_{\text{tot}} \approx b_{\text{ic}}$, and we arrive at the simple and important

result $q_{ic} \propto q_e$: the IC photon production rate is proportional to the electron injection rate. Physically, this arises because when IC losses dominate, the cosmic ray losses are directly probed by the gamma-ray signal we are calculating. Thus, the conservation of energy relates the portion of energy injected into cosmic-ray electrons to that later emitted as IC photons. Hence, the IC emission serves as an electron “calorimeter.” This limit is the case of perfect calorimetry, but in reality synchrotron and bremsstrahlung losses are also present and can be non-negligible. This is the case of partial or fractional calorimetry where $q_{ic}/q_e \propto b_{ic}/b_{tot}$: IC photons trace the portion of cosmic-ray energy lost via this mechanism (Pohl 1994). As we will see in greater detail in §4, IC losses are always important yet do not vastly overwhelm the other losses. Thus, calorimetry is only partially realised in detail. But even the approximate validity of calorimetry is sufficient that the IC gamma ray luminosity is a fairly robust calculation.

In the limit of perfect calorimetry, the IC volume emissivity is $q_{ic} \propto q_e$, and integration over all of the supernovae acting as cosmic-ray accelerators gives the IC luminosity $L_E \propto R_{SN} \propto \psi$. Physically, a fixed fraction of each supernova’s energy (and thus a fraction of each parcel of mass in new stars) goes into cosmic-ray electrons and ultimately into IC photons. This scaling can then be calibrated by GALPROP estimates for the total Milky-Way IC luminosity (Strong et al. 2010), which determines the IC output per unit star-formation. We can then find the luminosity for any star-forming galaxy at a fiducial energy of $E = 1$ GeV as,

$$\begin{aligned} E^2 L_E &= E^2 L_{E,MW} \left(\frac{\psi}{\psi_{MW}} \right) \\ &\approx 10^{40} \text{ GeV}^2 \text{ sec}^{-1} \text{ GeV}^{-1} \left(\frac{\psi}{1 M_\odot \text{ yr}^{-1}} \right) \end{aligned} \quad (5)$$

where ψ_{MW} is the Milky-Way star-formation rate.

From eqns. (1) (2), and (5), we estimate the IC contribution to the EGB intensity at 1 GeV as

$$\begin{aligned} E^2 I_E|_{ic,1 \text{ GeV}} &\approx \frac{L_{E,MW} n_{gal} d_H}{4 \pi} \left(\frac{\psi}{\psi_{MW}} \right) \approx \frac{L_{E,MW} d_H}{4 \pi \psi_{MW}} \dot{\rho}_*(1) \\ &\approx 3 \times 10^{-8} \text{ GeV cm}^2 \text{ sec}^{-1} \text{ sr}^{-1} \end{aligned} \quad (6)$$

where $\dot{\rho}_*(1) = \psi n_{gal} \approx 0.1 M_\odot \text{ yr}^{-1} \text{ Mpc}^{-3}$ is the cosmic star formation rate at $z = 1$ (Horiuchi et al. 2009). For comparison, the pionic model of Fields et al. (2010) gives an intensity $E^2 I_E|_{\pi \rightarrow \gamma\gamma, 1 \text{ GeV}} \sim 3 \times 10^{-7} \text{ GeV cm}^2 \text{ sec}^{-1} \text{ sr}^{-1}$, with a factor ~ 2 uncertainty in normalisation. The EGB measured by *Fermi* -LAT is $E^2 I_E|_{obs, 1 \text{ GeV}} = 6 \times 10^{-7} \text{ GeV cm}^2 \text{ sec}^{-1} \text{ sr}^{-1}$ (Abdo et al. 2010f). Thus, the pionic component alone dominates the overall amplitude from

the star-forming galaxies, which is an important contribution to the total observed flux. Not evident from our estimate is that the shape of the star-forming spectrum improves upon addition of the IC component, as we will see in §6.

3. Targets: Interstellar Photon Fields

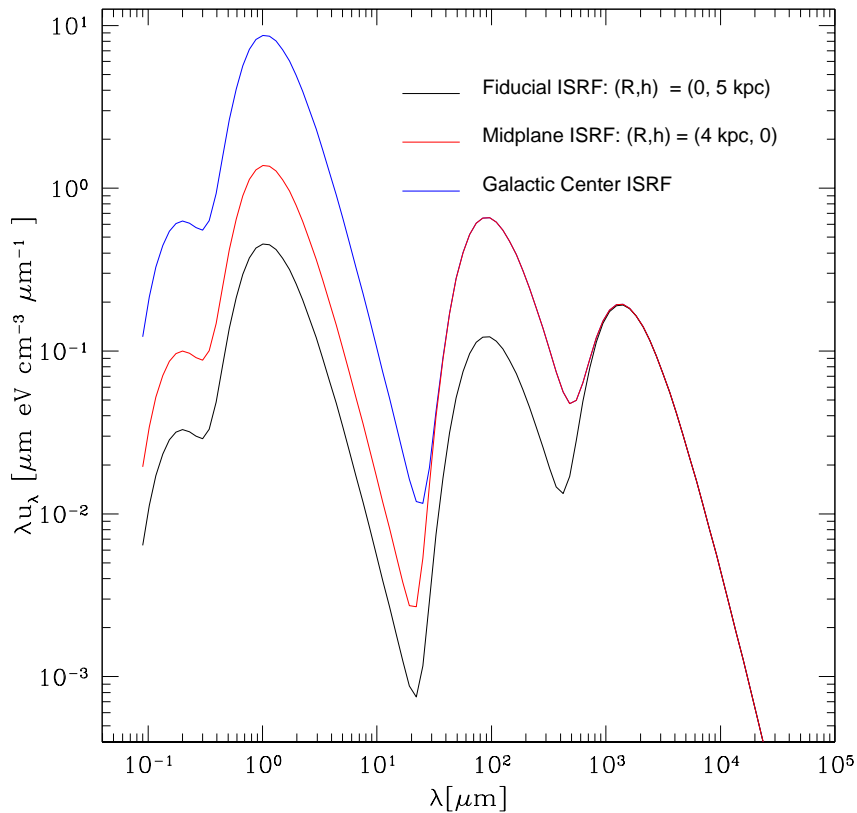


Fig. 1.— The interstellar photon field (ISRF) energy density, shown as a function of the wavelength. The model includes thermal components for starlight (optical), dust (IR) and the CMB as in Cirelli & Panci (2009). It includes another thermal component for the starlight in the UV. The black (fiducial), red and blue curves represent the curves for $(R, h) = (0, 5 \text{ kpc})$, $(4 \text{ kpc}, 0)$ and $(0, 0)$ respectively.

Cosmic-ray electrons in a galaxy will encounter a background photon field, commonly called the interstellar radiation field (ISRF). The ISRF is a rich function of both energy and geometry. We simplify this complex reality by treating a galaxy as a single zone for

the purposes of cosmic-ray propagation and gamma-ray emission. Thus, our ISRF is meant to give a sort of effective volume average of the radiation field encountered by cosmic-ray electrons. Our choice of ISRF follows those of models for the Milky Way, which we adjust at other cosmic epochs via scaling arguments. These scalings use the cosmic star formation rate $\dot{\rho}_*(z)$, whose change with redshift we characterize by the dimensionless function

$$S(z) \equiv \frac{\dot{\rho}_*(z)}{\dot{\rho}_*(0)} \quad (7)$$

where today $S(0) = 1$.

For the ISRF at the present day (redshift $z = 0$), we adopt but extend the model proposed by Cirelli & Panci (2009), which consists of three thermal components corresponding to the infra-red (or dust), optical, and the Cosmic Microwave Background (CMB). To this we add a fourth thermal component for the UV. Our goal is to build a simple model that can reproduce the inverse Compton luminosity of the Milky Way according to Strong et al. (2010); their calculation is based on a far more detailed, spatially-dependent ISRF as implemented in the GALPROP code (Strong et al. 2000; Porter et al. 2008). The strengths of the UV, IR and the optical relative to the CMB decreases with Galactocentric radial distance R and also with height h above the Galactic plane. This is seen in Fig. 1.

We may express the ISRF specific energy density $du_{\text{isrf}}/d\epsilon = \epsilon dn_{\text{isrf}}/d\epsilon$ as

$$\lambda \frac{du_{\text{isrf}}}{d\lambda} = \epsilon \frac{du_{\text{isrf}}}{d\epsilon} = \sum_{i=1}^4 f_i \frac{1}{\pi^2} \frac{\epsilon^4}{\exp(\epsilon/T_i) - 1} \quad (8)$$

a sum of Planck terms, with dimensionless weights f_i for the different background components: $i = \text{UV}$, optical, IR and the CMB. The UV and optical component are from starlight, and the IR comes from starlight reprocessed by dust. Our model, as seen in the Fig. 1 thus includes the effect of the major components in the GALPROP ISRF, which dominate the energy density. For the IR, we tried a non-thermal model that includes effect of both scattering and absorption by dust particles, but the effects on our gamma ray luminosity model are insignificant. Therefore, we retain the thermal model for IR. We also neglect the details at the optical-IR transition, where nonthermal lines appear but whose contribution to the energy density is sub-dominant.

Figure 1 shows our version of the ISRF at different locations in the Galaxy. The optical and dust components are taken from Cirelli & Panci (2009). We add another thermal component for the UV. The black, red and blue curves correspond to the positions $(R, h) = (0, 5)$, $(4, 0)$ and $(0, 0)$ kpc. The peaks due to starlight and IR change with position in the Galaxy, while the CMB contribution peaked at $\lambda \approx 1000$ microns remains the same. At the Galactic centre, the energy densities of these latter components are greater than the CMB, with

optical photons dominating. Above the Galactic plane, the CMB becomes comparable in energy density and eventually dominates at very large h .

Table 1 lists the temperatures of the various ISRF components along with their relative weights at zero redshift, $f_i(0)$. We chose the relative strengths for regions corresponding to $10^\circ < |b| < 20^\circ$ and $0^\circ < l < 360^\circ$, which corresponds to the ‘10-20’ model from Cirelli & Panci (2009) as our fiducial model. This is for the position $(R, h) = (0, 5)$ Kpc represented by the black curve in Fig. 1. The UV component at this position is scaled from that in the Galactic Centre, (Porter et al. 2008) in the same proportion as the optical component in these positions. This choice of model, with the overall normalisation adjusted, reproduces the Milky Way IC luminosity as a function of energy from Strong et al. (2010).

Table 1: ISRF Parameters

	UV	Optical	IR	CMB
fiducial $f_i(0)$	8.4×10^{-17}	8.9×10^{-13}	1.3×10^{-5}	1
Galactic Centre $f_i(0)$	1.6×10^{-15}	1.7×10^{-11}	7×10^{-5}	1
$T(0)$ [K]	1.8×10^4	3.5×10^3	41	2.73

Because we are interested in inverse Compton emission from star-forming galaxies over all of cosmic history, we must specify the cosmic evolution of the ISRF. This will depend on which stars contribute to starlight and dust scattered light. The detailed present-day Milky-Way model in Strong et al. (2000) uses the stellar luminosity functions from Wainscoat et al. (1992). The UV and IR components derive from short-lived massive stars, and the resulting starlight density will simply scale with the star-formation rate. Thus, we adopt the scalings

$$\begin{aligned}
 f_2(z) &= f_{\text{UV}}(z) = f_{\text{UV}}(0) S(z), \\
 f_3(z) &= f_{\text{IR}}(z) = f_{\text{IR}}(0) S(z)
 \end{aligned}
 \tag{9}$$

The optical component is less trivial and evolves differently for different stellar populations. Massive supernova progenitors, as well as AGB progenitors, are short-lived compared to $\gtrsim 1$ Gyr timescales for cosmic star formation. Consequently, the optical radiation density of these stars would scale as

$$f_2(z) = f_{\text{op}}(z) = f_{\text{op}}(0) S(z) \quad ,
 \tag{10}$$

in step with the UV and IR scaling. For reasonable initial mass functions and star-formation histories, these stars should dominate the optical ISRF. But for lower-mass main sequence stars and the red giants they become, their cosmologically long lifetimes mean that their starlight density at any epoch would scale as the integrated star-formation rate. Therefore,

their contribution to the optical component would scale as

$$f'_{\text{op}}(z) = f_{\text{op}}(0) \frac{\int_z^\infty dz \left| \frac{dt}{dz} \right| \dot{\rho}_\star}{\int_0^\infty dz \left| \frac{dt}{dz} \right| \dot{\rho}_\star} , \quad (11)$$

This would give a lower optical component and decrease the IC intensity as we will see. We will adopt eq. (10) for our fiducial model, but we will explore the effects of using eq. (11); these cases will bracket the true evolution.

The redshift dependence of the CMB is precisely known and can be expressed entirely in terms of its temperature,

$$T_{\text{CMB}}(z) = (1 + z) T_{\text{CMB}}(0) \quad (12)$$

with $f_4(0) = f_{\text{CMB}}(0) = 1$. The CMB energy density thus grows rapidly as $u_{\text{cmb}} \propto (1 + z)^4$.

4. Projectiles: Cosmic-Ray Electron Source and Propagation

An electron with energy $E_e = \gamma m$ scattering off a background photon of energy ϵ will produce IC photons with energies around $E_\gamma \sim \gamma^2 \epsilon$. In order to produce $E_\gamma \sim 100$ MeV to ~ 300 GeV gamma rays around the *Fermi* range, electrons with energies of few GeV to few TeV are required, depending on the energy of initial un-scattered photon. These are the electrons of interest to us.

High-energy cosmic ray electrons obey a complex transport equation (e.g., Strong et al. 2007). This in general would include effects of diffusion, convection, escape, radiative losses, etc. However, our approach is to create the simplest one-zone model that captures electron source spectrum and their most important losses.

We model cosmic-ray electron injection via the source spectrum from the Plain Diffusion (PD) model of Strong et al. (2010). In this model, electrons are accelerated with a broken power-law injection spectrum having $q_e(E_e) \propto E_e^{-1.8}$ up to a break at $E_{e,\text{break}} = 4$ GeV, and above this $q_e(E_e) \propto E_e^{-2.25}$. Electrons below $E_{e,\text{break}}$ can produce inverse Compton gamma rays at the low end of the *Fermi* range, when upscattering optical and UV photons. Gamma rays at higher energies are produced by electrons above the break energy. Thus, it is important to include the injection break in our calculations.¹

¹ Subsequent to the Strong et al. (2010) analysis of the global Milky Way luminosity, Strong et al. (2011) presented a revised electron injection spectrum that better fits new cosmic-ray electron data. They slightly change the power-law indices we have used, introduce a new spectral break at 50 GeV, and an exponential

With an interstellar diffusion coefficient, $D_0 \sim 10^{28} \text{cm}^2 \text{sec}^{-1}$ (Strong et al. 2010), the diffusion length for electrons over the Compton loss time-scales is $\ell_{\text{diff}} \sim 0.01 - 1$ kpc, depending on the energy. We thus see that electrons will not venture far from the Galaxy, but can range vertically outside the Galactic midplane. Hence, very few electrons will be lost to escape, in strong contrast to ions where escape dominates (Pohl 1994). We thus will ignore electron escape in our analysis.

However, since the electrons do propagate throughout and above the stellar and gaseous disk, the electron population sees a wide variety of radiation fields. Our single choice is a crude approximation meant to represent a sort of average ISRF. As a result, the electron propagation equation takes the “thick target” form

$$\frac{\partial}{\partial t} \phi_e(E_e) = q_e(E_e) + \frac{\partial}{\partial E_e} [b(E_e) \phi_e(E_e)] \quad (13)$$

where $q_e(E_e)$ is the source term and $b(E_e) = |dE_e/dt|$ is the total rate of energy loss. The equilibrium (i.e., $\partial_t \phi_e = 0$ steady state) solution of the cosmic ray flux is

$$\phi_e(E_e) = \frac{1}{b(E_e)} \int_{E_e}^{\infty} dE'_e q_e(E'_e) = \frac{q_e(> E_e)}{b(E_e)} \quad (14)$$

As usual in the thick-target limit, the electron flux is directly proportional to the energy-integrated injection rate $q_e(> E_e)$, and inversely proportional to the total energy loss rate. In general, the total energy loss rate of the electrons is given by sum of the inverse Compton, synchrotron, bremsstrahlung and ionisation losses,

$$b_{\text{tot}}(E_e) = b_{\text{ic}}(E_e) + b_{\text{sync}}(E_e) + b_{\text{brem}}(E_e) \quad ; \quad (15)$$

we now address each in turn. The ionisation loss is unimportant throughout the entire electron energy range of interest here.

The inverse Compton loss in the Thompson regime is given by the simple expression

$$\begin{aligned} b_{\text{ic}}(E_e) &\stackrel{\text{Thomps}}{=} \frac{4}{3} \sigma_{\text{T}} c U_{\text{isrf}} \left(\frac{E_e}{m c^2} \right)^2 \\ &\approx 1 \times 10^{-8} \text{ GeV sec}^{-1} \left(\frac{U_{\text{isrf}}}{1 \text{ eV cm}^{-3}} \right) \left(\frac{E_e}{10 \text{ TeV}} \right)^2 \end{aligned} \quad (16)$$

cutoff at 2 TeV. We have verified that, when keeping fixed the injection at the 4 GeV break, the Strong et al. (2011) spectrum does not strongly affect the overall IC amplitude, and over the *Fermi* EGB energy range the resulting IC luminosity is similar near 200 MeV, and slightly lower at higher energies.

However, the full Compton cross section takes the Klein-Nishina form described in more detail in §5.1. Corrections to the Thompson limit become important when $\Delta_\epsilon = 4 \epsilon \gamma / m c^2 \gg 1$; in a starlight-dominated ISRF with $\epsilon \sim 1$ eV, this occurs for electron energies $\gamma \gg 10^5$. This energy regime is important for our calculation and therefore, we calculate the inverse Compton loss rate by combining the Klein-Nishina cross section self-consistently with the (redshift-dependent) ISRF:

$$\begin{aligned}
 b_{\text{ic}}(E_e) &= \int_0^\infty d\epsilon \frac{dn_{\text{isrf}}(\epsilon)}{d\epsilon} \int dE_{\text{em}} (E_{\text{em}} - \epsilon) \frac{d\sigma_{\text{ic}}}{dE_{\text{em}}} \\
 &= 3 \sigma_{\text{T}} c \int_0^\infty d\epsilon \frac{dn_{\text{isrf}}(\epsilon)}{d\epsilon} \epsilon \int_{(m c^2/2E_e)^2}^1 dq \frac{(4 (\frac{E_e}{m c^2})^2 - \Delta_\epsilon)q - 1}{(1 + \Delta_\epsilon q)^3} \\
 &\quad \times \left(2q \ln(q) + (1 + 2q)(1 - q) + \frac{1}{2} \frac{(\Delta_\epsilon q)^2}{1 + \Delta_\epsilon q} (1 - q) \right) \quad (17)
 \end{aligned}$$

as in Cirelli & Panci (2009), where

$$q = \frac{E_{\text{em}}}{4\epsilon\gamma^2(1 - E_{\text{em}}/\gamma m c^2)} \quad (18)$$

Depending on the relative importance of the losses, the propagated electron spectrum changes (Felten 1965; Pohl 1993). For our fiducial ISRF model, the bremsstrahlung, synchrotron and Compton losses are all important, depending on the part of the spectrum. For electron energies lower than ~ 1 GeV, bremsstrahlung is dominant, with Compton losses being comparable close to the break energy at $E_e = 4$ GeV. Therefore, instead of seeing two breaks corresponding to these two cosmic ray propagation regimes, only one is seen near the break energy as described in §4.

Note also that for the highest-energy electrons, inverse Compton losses become catastrophic, i.e., in each scattering event the fractional changes in the electron energy approach $\delta E_e/E_e \sim 1$ (e.g., Blumenthal & Gould 1970). In this case the losses can no longer be treated as a smooth function $b_{\text{ic}}(E_e)$ that averages over many scatterings each with $\delta E_e/E_e \ll 1$; we do not include these effects, which impact gamma-ray energies of $E_{\text{em}} \gtrsim 1$ TeV.

The other energy loss rates are given as follows (Hayakawa 1973; Ginzburg 1979): synchrotron losses

$$\begin{aligned}
 b_{\text{sync}}(E_e) &= \frac{4}{3} \sigma_{\text{T}} c U_{\text{mag}} \left(\frac{E_e}{m c^2} \right)^2 = \frac{1}{6 \pi} \sigma_{\text{T}} c B^2 \left(\frac{E_e}{m} \right)^2 \\
 &\approx 3 \times 10^{-10} \text{ GeV sec}^{-1} \left(\frac{B}{1 \mu\text{G}} \right)^2 \left(\frac{E_e}{10 \text{ TeV}} \right)^2 \quad (19)
 \end{aligned}$$

are controlled by the interstellar magnetic energy density U_{mag} . The bremsstrahlung losses depend on whether the medium is ionised or neutral. Due to the presence of both H I and H

II, the bremsstrahlung losses are due to both neutral and ionised hydrogen (Hayakawa 1973; Ginzburg 1979):

$$b_{\text{brem}}(E_e) = b_{\text{brem,ion}}(E_e) + b_{\text{brem,n}}(E_e) \quad (20)$$

$$b_{\text{brem,ion}}(E_e) = \frac{3}{\pi} n_{\text{H II}} \alpha \sigma_{\text{T}} c E_e \left[\ln \left(\frac{2 E_e}{m c^2} \right) - \frac{1}{3} \right] \quad (21)$$

$$= 1.37 \times 10^{-12} \text{ GeV sec}^{-1} \left(\frac{n_{\text{H II}}}{1 \text{ cm}^{-3}} \right) \times \left(\frac{E_e}{10 \text{ TeV}} \right) \left[\ln \left(\frac{E_e}{10 \text{ TeV}} \right) + 17.2 \right] \quad (22)$$

$$b_{\text{brem,n}}(E_e) = \frac{3}{\pi} n_{\text{H I}} \alpha \sigma_{\text{T}} c E_e \left[\ln(191) + \frac{1}{18} \right] \quad (23)$$

$$= 7.3 \times 10^{-12} \text{ GeV sec}^{-1} \left(\frac{n_{\text{H I}}}{1 \text{ cm}^{-3}} \right) \left(\frac{E_e}{10 \text{ TeV}} \right) \quad (24)$$

Here $n_{\text{H I}}$ and $n_{\text{H II}}$ are the number density of relativistic electrons in the interstellar medium, which is equal to the number density of H I and H II.

Different loss mechanisms dominate at different energies. Inverse Compton losses scale as $b_{\text{ic}} \propto E_e^2$ in the Thompson regime, but for large E_e this drops off to a logarithmic energy dependence due to Klein-Nishina suppression. Synchrotron losses have $b_{\text{sync}} \propto E_e^2$, and thus are proportional to and are comparable to inverse Compton losses at moderate energies $E_e \sim 1 \text{ GeV} - \text{ TeV}$. At high electron energies, inverse Compton is suppressed and the synchrotron losses dominate. Below $E_e \sim 1 \text{ GeV}$, bremsstrahlung losses $b_{\text{brem}} \propto E_e$ become important.

The losses themselves evolve with redshift, through the dependences on interstellar densities, i.e., the ISRF energy density U_{isrf} , the interstellar magnetic energy density $U_{\text{mag}} = B^2/8\pi$, and the number densities n_{ism} of interstellar particles. The magnetic field couples to all cosmic rays, for which the ions dominate the energy density. This coupling is likely responsible for the approximate equipartition of magnetic field and cosmic-ray energy densities in the local interstellar medium. Therefore, we assume that the magnetic field energy density scales with the cosmic-ray ion flux, and therefore with the star-formation rate: $U_{\text{mag}} \propto S(z)$. For our fiducial model, we use $B_0 = 4 \mu \text{ G}$, to match the model of Strong et al. (2010), which is comparable with the typical value in Strong et al. (2011).

We take interstellar particle densities, which control bremsstrahlung losses, to scale as

$$n_i(z) = n_{i,0}(1+z)^3 \quad (25)$$

This can be viewed a consequence of the disk radius scaling $R_{\text{disk}} \propto (1+z)$ in the Fields et al. (2010) model, and to reflect proportionality between galaxy disk and dark halo sizes. The fiducial number densities of neutral and ionised hydrogen, i.e. $n_{\text{H II},0} = n_{\text{H I},0} = 0.06 \text{ cm}^{-3}$. The helium content of ionised and neutral gas is also included, with $y_{\text{He}} = 0.08$. These parameters are broadly consistent with values at intermediate heights h above the Galactic plane, as befits the volume average represented by our one-zone model. For reference, the values of n_{ism} and B used at the Galactic centre are much higher at $B_0 = 8.3 \mu\text{G}$ and $n_{\text{H II},0} = n_{\text{H I},0} = 0.12 \text{ cm}^{-3}$.

5. Inverse Compton Emission from Individual Star-Forming Galaxies

As seen in eq. (2), we first compute the luminosity of single galaxy and then average suitably over the luminosity function to get the luminosity density or cosmic volume emissivity. In this section, we address the former, focussing first on the IC emissivity *within* the volume of a single galaxy, then using this to compute the total luminosity from that galaxy.

5.1. Inverse Compton Emissivity of a Star-Forming Galaxy

The specific IC volume emissivity within a galaxy is the rate of producing gamma ray photons, $d\Gamma_{e^- \gamma \rightarrow e^- \gamma} / dE_{\text{em}}$ per background photon, multiplied by the ISRF number density, n_{isrf}

$$\frac{dq_\gamma}{dE_{\text{em}}} = \frac{dN_\gamma}{dV dE_{\text{em}} dt} = \int d\epsilon \frac{d\Gamma_{e^- \gamma \rightarrow e^- \gamma}}{dE_{\text{em}}} \frac{dn_{\text{isrf}}}{d\epsilon} . \quad (26)$$

Here, the gamma ray rate per unit ISRF photon is a product of the cosmic ray flux and the IC cross section

$$\frac{d\Gamma_{e^- \gamma \rightarrow e^- \gamma}}{dE_{\text{em}}} = \frac{d\sigma_{e^- \gamma \rightarrow e^- \gamma}}{dE_{\text{em}}} \phi_e . \quad (27)$$

that in general takes the Klein-Nishina form. The full Klein-Nishina cross section is a complicated function of the energies involved. Moreover, the inverse Compton process produces anisotropic emission if either the cosmic-ray or ISRF populations depart from isotropy. While the cosmic-ray electrons of interest are well-approximated as isotropic, in a real Galaxy the photon field is certainly anisotropic as well as spatially-varying. These effects are included in GALPROP (Moskalenko & Strong 2000), but we will ignore them in our simple one-zone galaxy model. This is a $\sim 20\%$ effect which will not dominate our final error budget.

For an electron with Lorentz factor $\gamma = E_e/m_e$, the Thompson limit is given as

$$4 \epsilon \gamma \ll mc^2 \quad (28)$$

For the electron spectra we consider, the Thompson limit is a good approximation for CMB and IR photons, but fails for UV and some optical photons. Hence, we use the Klein-Nishina result via the prescription of Jones (1968) and Blumenthal & Gould (1970). This differential cross section is expressed as,

$$\frac{d\sigma}{dE_{\text{em}}}(\epsilon, E_e, q) = \frac{3}{4} \frac{\sigma_{\text{T}}}{\epsilon \gamma^2} \left(2q \ln(q) + (1 + 2q)(1 - q) + \frac{1}{2} \frac{(\Delta_\epsilon q)^2}{1 + \Delta_\epsilon q} (1 - q) \right)$$

where σ_{T} is the total Thompson scattering cross section and q appears in eq. (18). In the Thompson limit, the last term in the above equation become negligible.

The inverse Compton volume emissivity within a one-zone galaxy is thus

$$\frac{dq_\gamma}{dE_{\text{em}}} = \int d\epsilon \frac{d\Gamma_{e^- \gamma \rightarrow e^- \gamma}}{dE_{\text{em}}} \frac{dn_{\text{isrf}}}{d\epsilon} = \int d\epsilon \frac{dn_{\text{isrf}}}{d\epsilon} \int dE_e \phi_e(E_e) \frac{d\sigma_{e^- \gamma \rightarrow e^- \gamma}}{dE_{\text{em}}} \quad (29)$$

We evaluate the emissivity numerically, by using the ISRF, cosmic ray flux density, and the cross section mentioned above, §3 and §4. That ISRF density n_{isrf} is the same as in the inverse Compton energy loss equation eq. (26), so that we calculate the two self-consistently.

It will be useful to cast the emissivity in the form

$$\frac{dq_\gamma}{dE_{\text{em}}} = U_{\text{isrf}} \frac{\int d\epsilon \frac{dn_{\text{isrf}}}{d\epsilon} \epsilon \left(\frac{1}{\epsilon} \frac{d\Gamma(\epsilon, E_{\text{em}})}{dE_{\text{em}}} \right)}{\int d\epsilon \frac{dn_{\text{isrf}}}{d\epsilon} \epsilon} \equiv U_{\text{isrf}} \left\langle \frac{1}{\epsilon} \frac{d\Gamma(\epsilon, E_{\text{em}})}{dE_{\text{em}}} \right\rangle = U_{\text{isrf}} \left\langle \frac{1}{\epsilon} \frac{q_e(> E_e)}{b} \frac{d\sigma}{dE_{\text{em}}} \right\rangle \quad (30)$$

where the angle brackets indicate an average weighted by the ISRF energy density distribution, and where the differential and total ISRF energy densities are $u_{\text{isrf}} = \epsilon \frac{dn_{\text{isrf}}}{d\epsilon}$ and $U_{\text{isrf}} = \int d\epsilon u_{\text{isrf}}$ respectively. We see that the amplitude of the emissivity scales as

$$q_\gamma \sim \frac{U_{\text{isrf}}}{b} q_e \sim \frac{b_{\text{ic}}}{b} q_e$$

Therefore, the photon emissivity, i.e., the gamma-ray source rate, is proportional to the electron source rate, but also depends on an appropriately weighted ratio of the inverse-Compton losses to the total losses. This ratio controls the shape of the spectrum. If the losses are Compton-dominated, then $b \sim b_{\text{ic}}$ and thus, the two source rates amplitudes are directly proportional, $q_\gamma \propto q_e$, and the IC emissivity is independent of the ISRF energy density, U_{isrf} . Thus, the number and energy of inverse Compton photons is proportional to that of cosmic-ray electrons, because in a steady state, the energy injected into electrons

must equal the energy emitted in IC photons. This situation defines perfect calorimetry. On the other hand, the ISRF *shape* in energy space is what weights the average in eq. (30), and thus the *shape* of the gamma-ray spectrum *does* remain sensitive to the ISRF even in the case of perfect calorimetry.

However, in reality, synchrotron and bremsstrahlung compete with inverse Compton losses at different energies, as seen in §4. In the Thompson regime, the ratio of synchrotron-to-inverse Compton losses

$$\frac{b_{\text{sync}}}{b_{\text{ic}}} \xrightarrow{\text{Thomps}} \frac{U_{\text{B}}}{U_{\text{isrf}}} = 0.4 \left(\frac{1.1 \text{ eV cm}^{-3}}{U_{\text{isrf}}} \right) \left(\frac{B}{4\mu\text{G}} \right)^2, \quad (31)$$

is energy-independent. For our fiducial magnetic field value, this ratio is not far from unity and hence, the shape does not change much for different parameters describing the ISRF and the magnetic field. On the other hand, for $E_e \gtrsim 1$ TeV, the IC losses are in the Klein-Nishina limit and grow only logarithmically in energy; then the synchrotron losses dominate. In this case, we have $q_\gamma \sim (U_{\text{isrf}}/U_{\text{mag}})q_e$. Thus, for high-energy cosmic-ray electrons, the calorimetric approximation increasingly breaks down.

The competition among losses depends on the way the interstellar densities evolve with redshift. Short-lived, massive stars dominate most of the ISRF except possibly for some of the optical range, and so the energy density scales with the star-formation rate $U_{\text{isrf}} \propto S(z)$. Due to cosmic-ray ion equipartition, we take $U_{\text{mag}} \propto S(z)$ as well, and thus the $U_{\text{isrf}}/U_{\text{mag}}$ ratio doesn't change dramatically throughout the cosmic history. Similarly, we also include a strong evolution $n_{\text{ism}} \propto (1+z)^3$ evolution to the interstellar particle density, which increases rapidly towards $z \sim 1$, roughly in step with the cosmic star-formation rate. Thus, the inverse-Compton/bremsstrahlung ratio of energy losses remains roughly constant as well out to $z \sim 1$. The net result is that the spectral shape of inverse Compton emission does not evolve dramatically with redshift in our model.

5.2. Total Inverse-Compton Luminosity from a Single Galaxy

As seen in §2, knowing the specific inverse Compton emissivity dq_γ/dE_{em} within a single star-forming galaxy, we can calculate the specific IC luminosity of the galaxy as

$$L_\gamma(E_{\text{em}}) = \frac{dN_{\gamma,\text{ic}}}{dt dE_{\text{em}}} = \int \frac{dq_\gamma}{dE_{\text{em}}} dV_{\text{ISM}} \quad (32)$$

and we have seen that $q_\gamma \propto (b_{\text{ic}}/b_{\text{tot}})q_e$. Following Fields et al. (2010), we take supernovae as the engines of cosmic-ray acceleration. Thus we scale the electron injection rate with

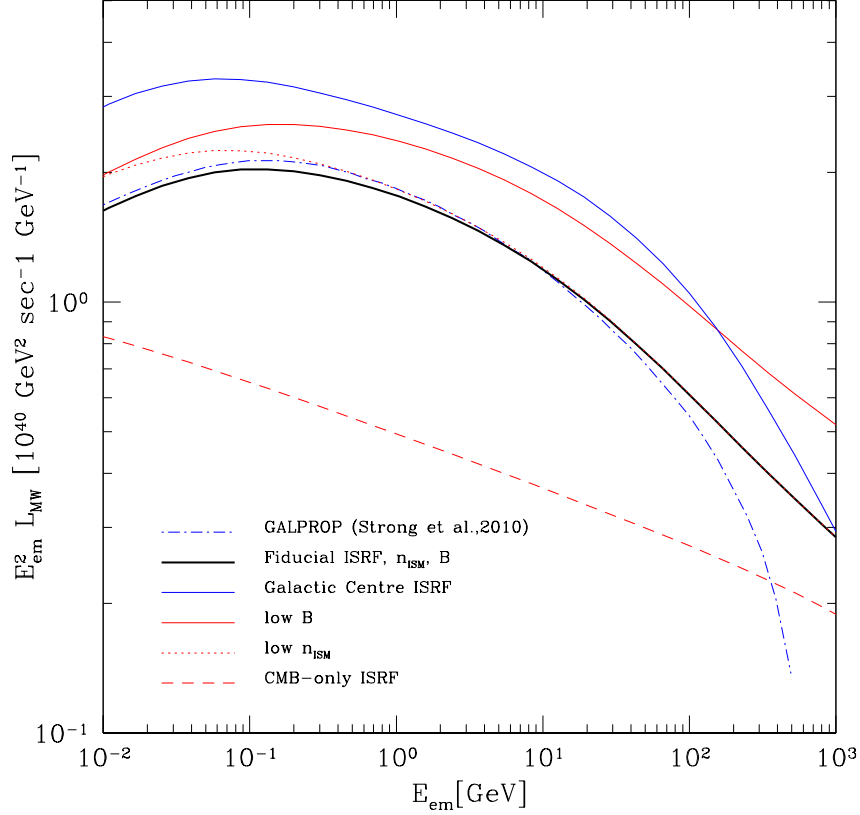


Fig. 2.— The inverse-Compton gamma-ray luminosity spectrum for a single galaxy with the Milky-Way star-formation rate. The solid black curve represents our fiducial model, with an ISM density $n_{\text{H I},0} = n_{\text{H II},0} = 0.06 \text{ cm}^{-3}$, magnetic field, $B_0 = 4 \mu\text{G}$. This is for the ISRF consistent with $(R, h) = (0, 5) \text{ kpc}$. This model is designed to provide a good fit to the GALPROP Plain Diffusion model of Strong et al. (2010, dot-dashed blue curve). The effect of some variations of gas density, magnetic field and ISRF are shown in red. The solid red curve shows the effect of reducing B to $2 \mu\text{G}$. The dotted red curve is for $n_{\text{H I},0} = n_{\text{H II},0} = 0.03 \text{ cm}^{-3}$. The red dashed is a toy model with the ISRF including the CMB alone. The solid blue shows the single galaxy template for the Galactic Centre, with $n_{\text{H I},0} = n_{\text{H II},0} = 0.12 \text{ cm}^{-3}$, and $B_0 = 8.3 \mu\text{G}$.

the supernova rate, i.e., we have $L_\gamma \sim \int q_e dV_{\text{ISM}} \propto R_{\text{SN}} \propto \psi$. This linear proportionality captures the main dependence of IC emission on star-formation rate.

Of course, in reality the cosmic ray flux and the ISRF are both functions of position in the galaxy. But we are describing a one-zone model, in which our choices of the fiducial parameters are made in order to provide the best match to the GALPROP Milky Way model in Strong et al. (2010). Specifically, we have created a best-fit model that mimics well the IC luminosity in the Strong et al. (2010) Plain Diffusion case. We adopt the same cosmic ray electron injection spectrum and amplitude, which are themselves chosen to provide a good fit to the observed local cosmic-ray electron spectrum. The interstellar parameters are the ISRF component amplitude f_i , the interstellar particle density n_{ism} , and the magnetic field strength B ; physically, these representing an average over the volume occupied by cosmic-ray electrons.

Thus, we have a single-galaxy IC luminosity that takes the separable form

$$L_\gamma(\psi, z) = \frac{\psi}{\psi_{\text{MW}}} L_{\text{MW}}(z) \quad (33)$$

where we have suppressed the energy dependence for clarity. Here we explicitly display the dominant sensitivity to star-formation, via the overall linear proportionality to the star-formation rate. The Milky-Way model $L_{\text{MW}}(z)$ is for a galaxy with the present-day Milky-Way star-formation rate, but allowing for redshift evolution of the interstellar matter and radiation densities.

Our IC luminosity models for $z = 0$ are shown in Fig. 2, along with that of Strong et al. (2010). Our fiducial model described in §3, §4 and §5.1 is represented by the solid black curve. The main feature of the inverse Compton $E_{\text{em}}^2 L_{\text{MW}}$ spectrum is that it has a broad maximum corresponding to the break in the electron injection spectrum at $E_{e,\text{break}} = 4$ GeV. In our the fiducial model, the optical component dominates the ISRF, and thus we expect the injection peak to correspond to an IC peak at $E_{\text{em}} \approx \gamma^2 \epsilon \approx 100$ MeV. This is about what our fiducial model predicts and is consistent with GALPROP.

Our fiducial model does a good job of reproducing the IC results of Strong et al. (2010), over most of the *Fermi* energy range. Thus, our results are equivalent to normalizing to the GALPROP luminosity for galaxies with the Milky Way’s star formation rate. We do not reproduce GALPROP’s steep decrease in the spectrum beyond 100 GeV, which may result from our neglect of the catastrophic nature of the electron energy losses in this regime. A fitting function for our fiducial IC model appears below in Table 2; the fit is good to better than 2% over the *Fermi* energy range. From this fit we see that at 1 GeV the logarithmic slope is around -0.1 , so that $L_{\text{MW}} \sim E_{\text{em}}^{-2.1}$. This is considerably flatter than both the pionic spectrum and the observed EGB at these energies.

Our choices of interstellar parameters for the fiducial model were made to provide a good fit to the GALPROP luminosity, and also are physically reasonable as volume averages. But of course other parameter choices are possible. To illustrate the sensitivity to these parameters, Fig. 2 shows variations of the luminosity with interstellar particle density n_{ism} and magnetic field strength B . Decreasing the gas density suppresses the bremsstrahlung losses relative to the total. This increases the ratio of $b_{\text{ic}}/b_{\text{brem}}$, which governs the IC spectral shape at lower energies. The result is a boost in the IC output at lower energies, which also shifts the IC peak towards lower energies. At high gamma-ray energies beyond $\sim \text{few GeV}$, synchrotron losses dominate, and thus the ratio $b_{\text{ic}}/b_{\text{sync}}$ controls the spectrum; reducing the magnetic field increases the luminosity.

The choice of ISRF is also important. Our fiducial model adopts an ISRF consistent with the GALPROP $(R, h) = (0, 5)$ kpc emission, as it best reproduces the IC luminosity of (Strong et al. 2010). If we change the ISRF to that of the Galactic centre, the IC signal is amplified, and the peak shifts to lower energies, as shown by the solid blue curve in Fig. 2. At the Galactic centre, the magnetic energy density is increased by a factor of 4 relative to the fiducial case, but the photon energy density goes up by more than a factor of 10. So both the fractions, b_{ic}/b and b_{sync}/b are higher, but so is $b_{\text{ic}}/b_{\text{sync}}$. And so the peak occurs at a lower energy, but has a greater amplitude. Finally, for illustration we turn off all components of the ISRF except the CMB, which substantially reduces the ISRF energy density and thus degrades calorimetry. We thus find that the overall signal is reduced and the peak shifts to far lower energies, as expected; indeed this peak is now off scale in Fig. 2. Of course, such a model is unphysical, because we are studying electrons born in star-forming systems where starlight is always present by definition.

Thus, there are several uncertainties in our simple model of the gamma ray spectrum for a single, Milky-Way like galaxy, such as choice of the average ISRF, the electron density, and the interstellar magnetic field. However, for reasonable interstellar models, these all lead to modest changes in the normalisation of the luminosity, at most tens of percent. Larger changes would be possible if one were to depart from the single galaxy template in Strong et al. (2010), which we try to reproduce and that is based on a wealth of Milky-Way data. Allowing oneself sufficient freedom, the inverse Compton EGB signal can be adjusted by changes, e.g., in the $U_{\text{isrf}}/U_{\text{B}}$ and $U_{\text{isrf}}/n_{\text{ism}}$ ratios that control the degree of electron calorimetry. Of course, this would then drive the system away from the rough energy equipartition observed in the Milky Way. Even then, large increases in these ratios would only increase the completeness of electron calorimetry and would raise the IC signal by a factor $\lesssim 2$; on the other hand, large decreases in these ratios would spoil calorimetry and could substantially lower the IC luminosity. Thus, the cosmological prediction of the IC contribution of the star-forming galaxies to the EGB should be fairly robust, unless there

are departures from the equipartition implicit in the Milky-Way-based normalization.

6. Results: Inverse Compton Contribution to the Extragalactic Background

Having established a one-zone galaxy template, and explored physically plausible variations in it, we proceed to compute the IC contribution to the EGB measured by *Fermi*-LAT from star-forming galaxies. This is given by the well-known expression

$$I_E = \frac{c}{4\pi} \int (1+z) \left| \frac{dt}{dz} \right| \mathcal{L}_\gamma[(1+z)E, z] dz \quad (34)$$

with $|dt/dz| = (1+z)^{-1} [(1+z)^3 \Omega_{\text{matter}} + \Omega_\Lambda]^{-1/2} H_0^{-1}$. Here we assume a flat Λ CDM universe with $H_0 = 71 \text{ km s}^{-1} \text{ Mpc}^{-1}$, $\Omega_{\text{matter}} = 0.3$, and $\Omega_\Lambda = 0.7$, following Fields et al. (2010).

The cosmic IC luminosity density (i.e., cosmic volume emissivity) is given by substituting our single-galaxy luminosity of eq. (33) into the luminosity function of eq. (2). Because we have $L_{\text{ic}} \propto \psi$, the IC emission of a star-forming galaxy traces its star-formation rate. Thus, the IC luminosity function $dn_{\text{gal}}/dL_\gamma$ at each redshift is proportional to the luminosity function of *any* tracer of star formation at that redshift. Suppressing the energy dependence for clarity, we have

$$\mathcal{L}_\gamma(z) = \int L_\gamma \frac{dn_{\text{gal}}}{dL_\gamma} dL_\gamma = \frac{L_{\text{MW}}(z)}{\psi_{\text{MW}}} \int \psi \frac{dn_{\text{gal}}}{dL_\gamma} dL_\gamma \quad (35)$$

$$= \frac{\dot{\rho}_\star(z)}{\psi_{\text{MW}}} L_{\text{MW}}(z) = S(z) \frac{\dot{\rho}_\star(0)}{\psi_{\text{MW}}} L_{\text{MW}}(z) \quad (36)$$

where the $\dot{\rho}_\star = \langle \psi n_{\text{gal}} \rangle = \int \psi dn_{\text{gal}}/dL_\gamma dL_\gamma$ is the cosmic star-formation rate. Following Fields et al. (2010) we adopt the Horiuchi et al. (2009) cosmic star-formation rate, and a Milky Way star-formation rate $\psi_{\text{MW}} = 1.07 M_\odot/\text{yr}$ (Robitaille & Whitney 2010).

The overall amplitude of the cosmic IC luminosity density is thus linearly proportional to the cosmic star-formation rate. Of course, the detailed spectral shape of the luminosity density reflects redshift dependence of the interstellar matter and radiation encoded in $L_{\text{MW}}(z)$.

Figure 3 shows the IC contribution to the EGB for several choices of the Milky-Way spectrum L_{MW} . The results for the fiducial model appear as the solid black curve, and incorporate the full redshift-dependence of interstellar density encoded in $L_{\text{MW}}(z)$. A fitting function for the fiducial model appears in Table 2, valid over the *Fermi* energy range. For comparison, Fig. 3 shows the pionic contribution in red. The IC contribution is about 10%

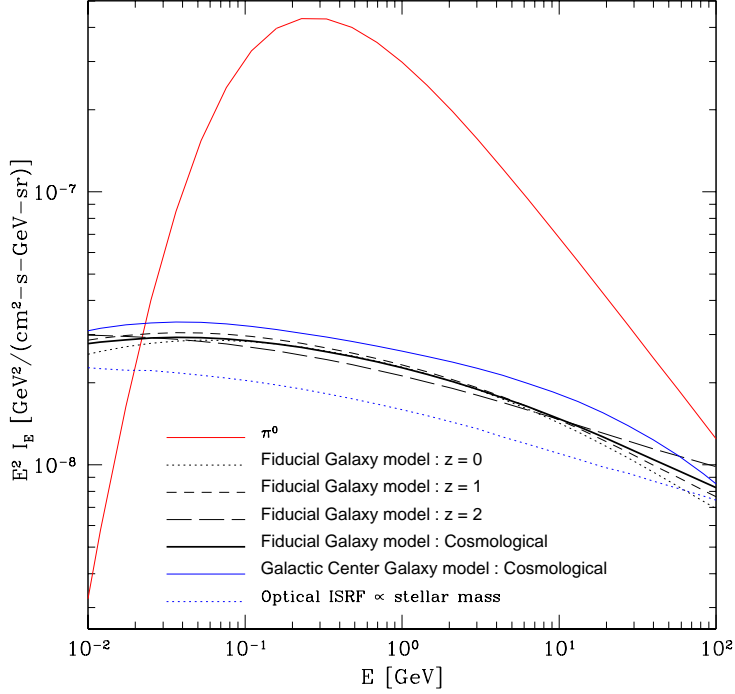


Fig. 3.— The inverse-Compton EGB intensity from star-forming galaxies as a function of energy. The solid black curve represents our fiducial IC model, using a single-galaxy model where interstellar densities evolve with redshift. The dotted and the dashed curves show the single galaxy template that does not evolve but is fixed to the behavior at $z = 0, 1$ and 2 . The solid blue curve is for an evolving single galaxy template with an ISRF corresponding to the Galactic centre model. The dotted blue shows the effect of scaling the optical ISRF with the cosmic stellar mass density (eq. 11). The red curve shows the pionic signal from normal star-forming galaxies as in Fields et al. (2010).

of the pionic contribution at the ~ 300 MeV peak in E^2I ; growing to about 20% at 10 GeV. This is consistent with our expectations from the order-of magnitude calculations of §2.

The shape of the IC curve is rather smooth, and rather flat in E^2I . This is because the spectrum it is a redshift-smearred version of the single-galaxy IC emission. This stands in contrast to the pionic curve that displays its characteristic peak and a steep $\sim E^{-s_p}$ dropoff at large energies, with $s_p = 2.75$ the propagated proton spectral index.

We have verified that the bulk of the IC signal comes from redshifts around $\bar{z} \sim 1$. That is, the integrand in eq. (34) peaks in this regime. A comparison of the corresponding curves in Figs. 2 and 3 shows that the IC peak in the galaxy luminosity rest-frame energy $E_{\text{em}} \simeq 100$ MeV is transformed into an EGB IC peak at $\simeq 40$ MeV. This translation in energy space is consistent with redshifting by a factor $1 + \bar{z}$.

The sensitivity to the interstellar density evolution adopted in our fiducial model is explored by the dashed and dotted black curves in Fig. 3. These show the effect of assuming a single galaxy spectral template that does not evolve with redshift, but rather at all epochs uses non-evolving interstellar densities corresponding to our model $L_{\text{MW}}(z_0)$ evaluated at some fixed redshift z_0 . Results are shown for this non-evolving source spectrum fixed for the entire cosmic history to the spectrum for redshifts $z_0 = 0, 1$ and 2 . It is clear that the actual cosmological result shown by the solid black curve is closest to the $z_0 = 1$ case, where the bulk of the IC signal originates. Moreover, we see that all of the single-redshift source spectra lead to EGB spectra very similar to the fiducial evolving $L_{\text{MW}}(z)$. This reflects the insensitivity of our source spectrum with redshift, which itself arises due to calorimetry and the near-constancy of the $U_{\text{isrf}} : U_{\text{mag}} : n$ density ratios.

To give a sense of the effect of the adopted ISRF, we have computed the IC EGB resulting from an evolving ISRF whose spectral shape is appropriate for the Galactic centre. This model corresponds to the solid blue curve in Fig. 2. Here again, the main result is that the curves are very similar. In detail, the Galactic centre has a slightly higher ratio $U_{\text{isrf}}/U_{\text{mag}}$ of starlight-to-magnetic energy density. Thus, electron energy losses are more IC dominated, and finally the overall IC flux is closer to calorimetric and so slightly higher.

Our fiducial model assumes the ISRF components (other than the CMB) are dominated by short-lived stars and thus have a redshift evolution that scales with the cosmic star-formation rate. An extreme alternative is that the optical ISRF is dominated by long-lived main sequence stars whose energy density scales with the stellar mass and thus the integrated cosmic star-formation rate, as in eq. (11). The dotted curve in Fig. 3 shows the EGB for this case. The signal is somewhat smaller than the fiducial model across all energies. This is easily understood: at high redshifts the star-formation rate is higher than today, but the

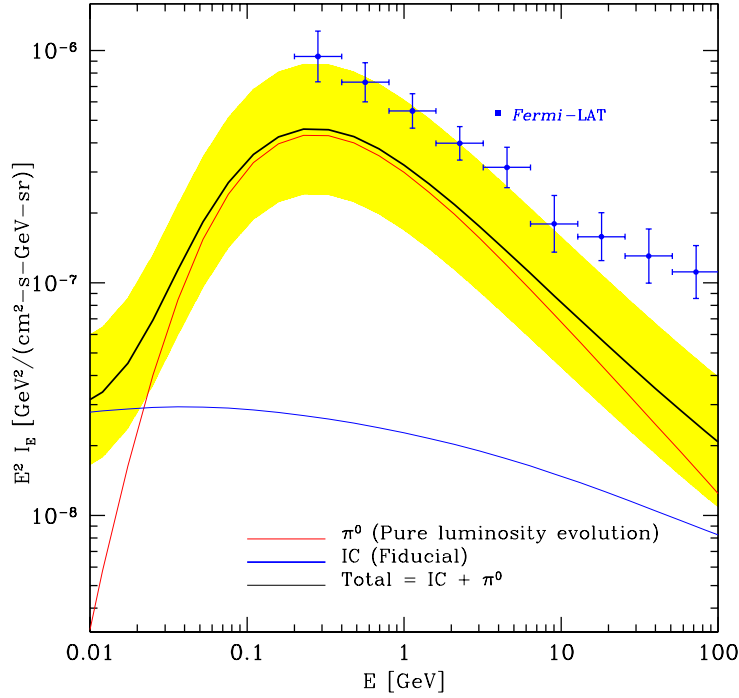


Fig. 4.— A summary of the star-forming galaxy contributions to the EGB intensity, shown as a function of energy. The blue points represent the *Fermi*-LAT data points (Abdo et al. 2010f). The solid red and blue curves show the gamma ray intensity due to pionic and fiducial IC components from star-forming galaxies as in Fig. 3. The solid black curve represents the sum of the two. The shaded band gives our estimate of the uncertainty in the predicted total signal, which is dominated by systematic errors that are common to the IC and pionic components.

stellar mass is lower and thus offers less optical photons and reduced calorimetry. But the effect is not dramatic; even in this extreme case, the reduction in the IC signal is less than a factor of two relative to our fiducial model.

Thus, we see that the IC results do depend on the adopted interstellar densities and their redshift evolution. But for reasonable choices, the variations in the final IC EGB result are small. The IC calculation in this sense appears rather robust to the systematic uncertainties in the modeling.

It is useful to compare the IC luminosity density in eq. (36) with that for pionic emission. As noted above, the cosmic IC emissivity is proportional to the cosmic star-formation rate, along with a weak sensitivity to the redshift evolution of interstellar densities. In contrast, the Fields et al. (2010) pionic emission depends on the product of cosmic star-formation rate and mean interstellar gas mass, via the nonlinear scaling $L_\pi \sim \psi^{1+\omega}$ with $\omega = 0.714$. Thus, the pionic emissivity represents a different moment of the cosmic star-formation rate $\mathcal{L}_\pi = \langle L_\pi n_{\text{gal}} \rangle \sim \langle \psi^{1+\omega} n_{\text{gal}} \rangle$. This nonlinear moment gives different results depending on how the star-formation distribution evolves with redshift. Two extreme limits correspond to: (a) pure density evolution, wherein galaxies have constant star-formation rates but evolving number density; versus (b) pure luminosity evolution in which the star-forming galaxy density is constant but the star-formation rates all evolve with redshift. The pionic curves we show correspond to the fiducial Fields et al. (2010) pure luminosity evolution case, which gives a contribution to the EGB larger by a factor ~ 3 than in the pure density evolution case. In the IC calculation, the pure luminosity and pure density evolution are degenerate, in that these models all give the same cosmic star-formation rate and thus the same IC output.

Figure 4 represents the central result of this paper, summarizing the EGB predictions for gamma-ray emission from star-forming galaxies in the *Fermi* energy range. We show the fiducial IC curve from Fig. (3), the fiducial normal-galaxy pionic model of Fields et al. (2010), and the total EGB intensity that sums these components. Over the 100 MeV to 300 GeV range, the pionic component dominates the normal galaxy contribution. But as we have seen, the IC curve is a much flatter function of energy. The IC component thus becomes systematically more important at higher energies. Consequently, high-energy slope of the total emission is less steep than that of the pionic signal, and closer to the *Fermi*-LAT data shown in blue (Abdo et al. 2010f).

Including the IC emission thus improves the agreement between star-forming prediction and the observed EGB slope, which had been a weaker point of the Fields et al. (2010) pionic-only model. Up to about ~ 10 GeV, the central values of the model fall below the data, but are consistent within the theoretical and observational error budget (discussed below). At higher energies, the model underpredicts the data. Our pionic model neglects

starburst galaxies; it may well be that their pionic emission is important at this energy range (e.g., Lacki et al. 2011). In addition, unresolved blazars are also guaranteed to play a role (e.g., Stecker & Venters 2011). In any case, star-forming galaxies clearly are an important contribution to the *Fermi* EGB signal, and could well be the dominant component.

Note also that the IC curve does not become important at *low* energies until far below the pion bump. Thus, the Fields et al. (2010) conclusions stand: the pion feature should still remain as a distinguishing characteristic of a significant star-forming contribution to the EGB. Measurements below ~ 200 MeV should show a break in the EGB slope if star-forming galaxies play an important role. Such a spectral feature provides one way to discriminate between star-forming galaxies and other sources, such as the guaranteed contribution from unresolved blazars.

Table 2: Fitting Functions

Form: $Y = 10^{aX^3+bX^2+cX+d}$, with $X = \log_{10}(E/1 \text{ GeV})$					
	Y	a	b	c	d
$E_{\text{em}}^2 L_{\text{ic}}(E_{\text{em}})$	[GeV s $^{-1}$]	-4.75×10^{-3}	-6.22×10^{-2}	-0.121	40.252
$E^2 I_{\text{ic}}(E)$	[GeV cm $^{-2}$ s $^{-1}$ sr $^{-1}$]	5.03×10^{-3}	-4.31×10^{-2}	-0.150	-7.64

Our estimate of the uncertainty in the total normal galaxy emission is represented by the shaded band in Figure 4. The errors in the pionic contribution dominate, and are taken from Fields et al. (2010). For the IC contribution, the errors are dominated by systematic uncertainties in the Milky-Way star formation rate ψ_{MW} and in the normalization $\dot{\rho}_{\star}(0)$ of the cosmic star-formation rate. These factors are common to the overall normalizations of *both* the pionic and IC signals, cf. eq. (36). Hence, the addition of the IC signal to the total does not substantially increase the error budget, and so we have retained the uncertainty band of Fields et al. (2010). The errors as shown are slightly underestimated at the highest energies, but we will see that other effects enter at this regime.

We have ignored the effect of intergalactic absorption of the high-energy gamma rays via $\gamma\gamma_{\text{ebl}} \rightarrow e^+e^-$ photo-pair production in collisions with extragalactic background light (e.g., Salamon & Stecker 1998; Abdo et al. 2010c; Stecker et al. 2012). This attenuation starts to become significant for gamma rays over few tens of GeV. Therefore, beyond these energies our results will be suppressed by amounts that depend on the optical depth for these high-energy gamma rays. In this context it is worth noting that *Fermi*-LAT observations of the $z = 0.9$ active galaxy, 4C +55.17 do not show significant absorption of gamma rays up to

about 100 GeV (McConville et al. 2011). This object lies within the $z \sim 1$ regime where most of the IC contribution to the EGB occurs; thus we might expect that attenuation should be mild at *Fermi* energies.

7. Discussion and Conclusions

We have calculated the contribution to the extragalactic gamma-ray background due to inverse-Compton emission from star-forming galaxies. To do this we model the IC emission in individual star-forming galaxies, which arises from cosmic-ray electron interactions with the ISRF. We normalize to the present-day Milky Way IC luminosity as determined by GALPROP (Strong et al. 2010). Indeed, we hope our simplified models helps to illuminate some of the rich physics in the GALPROP model. We also provide a prescription for redshift evolution of interstellar matter and energy densities, based on equipartition arguments. Assuming cosmic rays are accelerated by supernovae implies that a galaxy’s IC luminosity scales as $L_{\text{ic}} \propto \psi$; this further implies that the cosmic IC luminosity density or volume emissivity is proportional to the cosmic star-formation rate: $\mathcal{L}_\gamma \propto \dot{\rho}_*$.

This linear dependence of IC luminosity with star-formation rate has important implications in light of the star-forming galaxies *resolved* by *Fermi*. Namely, the $L_{\text{ic}} \propto \psi$ trend provides a poor fit for *Fermi* galaxies, for which the observed correlation is non-linear: $L_{\text{ic}} \propto \psi^{1.4 \pm 0.3}$ (e.g., Abdo et al. 2010d). This implies that the IC component is subdominant in *Fermi* galaxies, adding indirect evidence for the primacy of pionic emission in star-forming galaxies and prefiguring the trends we find for the EGB.

Turning to the EGB, we find that the IC contribution has a very broad maximum in $E^2 I_{\text{ic}}$ at $E \simeq 40$ MeV, falling off very gradually away from this peak. This shape is a redshift-smearred reflection of the underlying Milky-Way-like spectrum from the individual galaxies. In fact, the IC emission is so broadly peaked that is it effectively featureless. This contrasts markedly with the distinctive pionic feature from cosmic-ray hadronic interactions in star-forming galaxies.

The amplitude and shape of the IC contribution to the EGB depends on the nature of the interstellar radiation and matter fields, and their evolution with redshift. However, we find that when we adopt different but physically motivated variations to our fiducial model, the final EGB predictions change very little. This rough model-independence of the IC EGB is a consequence of partial calorimetry, i.e., the fact that IC photons represent a substantial fraction of cosmic-ray electron energy loss, so that the IC output is tied to cosmic-ray production via energy conservation.

We find that in all of our models, the IC signal is always smaller than the pionic contribution from normal galaxies. This largely follows from our normalization to the Milky Way emission, where the GALPROP model finds (and *Fermi* observations imply) that pionic emission dominates over IC. However, while the EGB IC component is smaller, it also has a substantially flatter spectrum, so that the IC becomes increasingly important away from the pionic peak. This implies that, at least for normal star-forming galaxies, the IC contribution should dominate over pionic at high and low energies. However, at higher energies the opacity of the universe becomes important and losses become catastrophic, and requires different techniques to handle correctly. At energies below the *Fermi*-LAT range, the IC emission will be supplemented by processes such as bremsstrahlung, which we have not included; a detailed treatment of the MeV regime appears in Lacki et al. (2012).

The approximate calorimetric relationship between IC photons and cosmic-ray electrons has important consequences. One is that as long as cosmic-ray electrons are accelerated with similar spectra and efficiency everywhere, their resulting IC emission will not depend strongly on their environment. For this reason, we expect that the IC output per supernova should be the same for normal galaxies and starburst galaxies, at least to zeroth order. This would mean that, unlike the pionic case, the IC emission from all star-forming galaxies can be treated on the same footing. Thus, we have not excluded starbursts in our analysis, as they were from the pionic signal. If we did so it would only reduce the overall IC signal from normal galaxies to even less than the pionic contribution.

Another consequence of partial calorimetry is that the main redshift dependence of the cosmic IC emissivity is a linear dependence on the cosmic star-formation rate. Thus, our results are independent of whether the cosmic star-formation rate is a result of pure luminosity evolution, pure density evolution, or something in between. This is in contrast to the pionic case, which depends nonlinearly on the star-formation luminosity function and so breaks the degeneracy between the pure luminosity and pure density evolution cases.

To simplify the discussion, the IC and pionic models presented here neglected the effects of Type Ia supernovae, implicitly assuming instead that all supernovae in star-forming galaxies are due to core-collapse. Lien & Fields (2012) considered in detail the effect of Type Ia supernovae on the pionic signal. They found that a self-consistent treatment includes both the addition of Type Ia explosions as cosmic-ray accelerators, but also as part of the Milky-Way normalization of the cosmic-ray/supernova ratio. The effects largely cancel, so that in the end, the net pionic galactic luminosity and EGB does not change substantially. In the case of IC emission a similar cancellation will occur. The only new contribution of possible importance comes from Type Ia explosions arising from long-lived progenitors in quiescent (i.e., not actively star-forming) galaxies such as ellipticals; the pionic emission from these

systems could be large if they have a substantial reservoir of hot, X-ray-emitting gas. But supernova rate in these galaxies represents a subdominant fraction of cosmic Type Ia activity, which itself is substantially smaller than the cosmic core-collapse rate. Thus, the IC contribution from these systems will be small. And so inclusion of Type Ia supernovae in a self-consistent way would change our results very little, less than the uncertainties in the model.

To our knowledge, this paper present the first discussion of the IC contribution from star-forming galaxies to the EGB.² There remains room to improve on our model. Future work would benefit from observational progress in clearly identifying an IC signal from individual star-forming galaxies, at energies away from the pionic peak. Theoretical work would benefit from a more detailed model for the ISRF and its evolution, and from the use of additional multiwavelength constraints on the cosmic ray electrons.

More broadly, a solid identification and quantification of the main components of the EGB remains a top priority for gamma-ray astrophysics and particle cosmology. Extending the *Fermi* EGB energy spectrum to both higher and lower energies will provide important new constraints. At sufficiently high energies, the cosmic opacity due to photo-pair production must become apparent if the EGB is dominated by *any* sources at cosmological distances (e.g., Salamon & Stecker 1998; Abdo et al. 2010c; Stecker et al. 2012). And at energies just below those reported in Abdo et al. (2010f), a break in the EGB spectrum is an unavoidable prediction if the signal is dominantly unresolved pionic emission from star-forming galaxies (both normal and starbursts). An independent probe of EGB origin lies in anisotropy studies (Ando & Komatsu 2006; Ando & Pavlidou 2009; Hensley et al. 2010; Ackermann et al. 2012; Malyshev & Hogg 2011). Regardless of the outcome, an assay of the EGB components will provide important new information (and perhaps some surprises!) about the high-energy cosmos.

It is a pleasure to acknowledge stimulating conversations with Vasiliki Pavlidou, Tijana Prodanović, Amy Lien and Todd Thompson. BDF would also like to thank the participants of the 2012 Sant Cugat Forum on Astrophysics for many lively and enlightening discussions. This work was partially supported by NASA via the Astrophysics Theory Program through award NNX10AC86G.

² As we were in the final stage of preparing this paper, we became aware of the work of Lacki et al. (2012) which addresses similar issues.

REFERENCES

- Abazajian, K. N., Blanchet, S., & Harding, J. P. 2011, *Phys. Rev. D*, 84, 103007
- Abdo, A. A., Ackermann, M., Ajello, M., et al. 2009, *Physical Review Letters*, 103, 251101
- . 2010a, *ApJ*, 709, L152
- . 2010b, *A&A*, 523, A46
- . 2010c, *ApJ*, 723, 1082
- . 2010d, *A&A*, 523, L2
- . 2010e, *A&A*, 512, A7
- . 2010f, *Physical Review Letters*, 104, 101101
- Ackermann, M., Ajello, M., Albert, A., et al. 2012, *Phys. Rev. D*, 85, 083007
- Ahlers, M., Mertsch, P., & Sarkar, S. 2009, *Phys. Rev. D*, 80, 123017
- Ando, S., & Komatsu, E. 2006, *Phys. Rev. D*, 73, 023521
- Ando, S., Komatsu, E., Narumoto, T., & Totani, T. 2007, *Phys. Rev. D*, 75, 063519
- Ando, S., & Pavlidou, V. 2009, *MNRAS*, 400, 2122
- Bignami, G. F., Fichtel, C. E., Hartman, R. C., & Thompson, D. J. 1979, *ApJ*, 232, 649
- Blumenthal, G. R., & Gould, R. J. 1970, *Reviews of Modern Physics*, 42, 237
- Brecher, K., & Morrison, P. 1967, *ApJ*, 150, L61
- Bringmann, T., Donato, F., & Lineros, R. A. 2012, *J. Cosmology Astropart. Phys.*, 1, 49
- Cirelli, M., & Panci, P. 2009, *Nuclear Physics B*, 821, 399
- Faucher-Giguère, C.-A., & Loeb, A. 2010, *J. Cosmology Astropart. Phys.*, 1, 5
- Felten, J. E. 1965, *Physical Review Letters*, 15, 1003
- Felten, J. E., & Morrison, P. 1963, *Physical Review Letters*, 10, 453
- Fichtel, C. E., Hartman, R. C., Kniffen, D. A., et al. 1975, *ApJ*, 198, 163
- Fields, B. D., Pavlidou, V., & Prodanović, T. 2010, *ApJ*, 722, L199

- Geringer-Sameth, A., & Koushiappas, S. M. 2012, MNRAS, 421, 1813
- Ginzburg, V. L. 1979, Theoretical physics and astrophysics (Oxford: Pergamon)
- Hayakawa, S. 1973, Cosmic ray physics: nuclear and astrophysical aspects. (Moskva:Mir)
- Hayakawa, S., Ito, K., & Terashima, Y. 1958, Progress of Theoretical Physics Supplement, 6, 1
- Hayakawa, S., Okuda, H., Tanaka, Y., & Yamamoto, Y. 1964, Progress of Theoretical Physics Supplement, 30, 153
- Helder, E. A., Vink, J., Bassa, C. G., et al. 2009, Science, 325, 719
- Hensley, B. S., Siegal-Gaskins, J. M., & Pavlidou, V. 2010, ApJ, 723, 277
- Horiuchi, S., Beacom, J. F., & Dwek, E. 2009, Phys. Rev. D, 79, 083013
- Jones, F. C. 1968, Physical Review, 167, 1159
- Kennicutt, Jr., R. C. 1998, ApJ, 498, 541
- Kraushaar, W. L., Clark, G. W., Garmire, G. P., et al. 1972, ApJ, 177, 341
- Lacki, B. C., Horiuchi, S., & Beacom, J. F. 2012, ArXiv, submitted
- Lacki, B. C., Thompson, T. A., & Quataert, E. 2010, ApJ, 717, 1
- Lacki, B. C., Thompson, T. A., Quataert, E., Loeb, A., & Waxman, E. 2011, ApJ, 734, 107
- Lenain, J.-P., & Walter, R. 2011, A&A, 535, A19
- Lien, A., & Fields, B. D. 2012, ArXiv e-prints
- Loeb, A., & Waxman, E. 2000, Nature, 405, 156
- Makiya, R., Totani, T., & Kobayashi, M. A. R. 2011, ApJ, 728, 158
- Malyshev, D., & Hogg, D. W. 2011, ApJ, 738, 181
- McConville, W., Ostorero, L., Moderski, R., et al. 2011, ApJ, 738, 148
- Miniati, F. 2002, MNRAS, 337, 199
- Moskalenko, I. V., & Porter, T. A. 2009, ApJ, 692, L54
- Moskalenko, I. V., & Strong, A. W. 2000, ApJ, 528, 357

- Murphy, E. J., Porter, T. A., Moskalenko, I. V., Helou, G., & Strong, A. W. 2012, *ApJ*, 750, 126
- Nolan, P. L., Abdo, A. A., Ackermann, M., et al. 2012, *ApJS*, 199, 31
- Pavlidou, V., & Fields, B. D. 2001, *ApJ*, 558, 63
- . 2002, *ApJ*, 575, L5
- Persic, M., & Rephaeli, Y. 2010, *MNRAS*, 403, 1569
- . 2011, ArXiv e-prints
- . 2012, ArXiv e-prints
- Pohl, M. 1993, *A&A*, 270, 91
- . 1994, *A&A*, 287, 453
- Porter, T. A., Moskalenko, I. V., Strong, A. W., Orlando, E., & Bouchet, L. 2008, *ApJ*, 682, 400
- Robitaille, T. P., & Whitney, B. A. 2010, *ApJ*, 710, L11
- Salamon, M. H., & Stecker, F. W. 1998, *ApJ*, 493, 547
- Sreekumar, P., Bertsch, D. L., Dingus, B. L., et al. 1998, *ApJ*, 494, 523
- Stecker, F. W., Malkan, M. A., & Scully, S. T. 2012, ArXiv e-prints
- Stecker, F. W., & Venters, T. M. 2011, *ApJ*, 736, 40
- Strong, A. W., Moskalenko, I. V., & Ptuskin, V. S. 2007, *Annual Review of Nuclear and Particle Science*, 57, 285
- Strong, A. W., Moskalenko, I. V., & Reimer, O. 2000, *ApJ*, 537, 763
- Strong, A. W., Orlando, E., & Jaffe, T. R. 2011, *A&A*, 534, A54
- Strong, A. W., Porter, T. A., Digel, S. W., et al. 2010, *ApJ*, 722, L58
- Strong, A. W., Wolfendale, A. W., & Worrall, D. M. 1976a, *Journal of Physics A Mathematical General*, 9, 1553
- . 1976b, *MNRAS*, 175, 23P

Torres, D. F., Reimer, O., Domingo-Santamaría, E., & Digel, S. W. 2004, *ApJ*, 607, L99

Uchiyama, Y., Aharonian, F. A., Tanaka, T., Takahashi, T., & Maeda, Y. 2007, *Nature*, 449, 576

Wainscoat, R. J., Cohen, M., Volk, K., Walker, H. J., & Schwartz, D. E. 1992, *ApJS*, 83, 111

Webber, W. R., Simpson, G. A., & Cane, H. V. 1980, *ApJ*, 236, 448